Theory of photon Bloch oscillations in photonic crystals

G. Malpuech,[1] A. Kavokin,[1] G. Panzarini,[2] and A. Di Carlo[3]
[1]*LASMEA, UMR No. 6602 du CNRS, Université Blaise Pascal–Clermont-Ferrand II, 63177 Aubière Cedex, France*
[2]*INFM, Dipartimento di Fisica ''A. Volta,'' Università di Pavia, Via Bassi, I-27100, Pavia, Italy*
[3]*INFM, Dipartimento di Ingegneria Elettronica, Università di Roma II ''Tor Vergata,'' Via Tor Vergata s.n.c., 00133, Roma, Italy*
(Received 7 July 2000; published 2 January 2001)

We study photonic Bloch oscillations (PBO's) in various quasiperiodic dielectric structures. Photons, like electrons, may experience confinement within inclined allowed optical bands of photonic structures, which results in a characteristic photonic Wannier-Stark ladder (PWSL) and PBO's analogous to electronic Bloch oscillations in crystals subjected to an electric field. In the photonic case the role of the electric field is played by a gradient of the size of the elementary cell of the optical crystal. The photonic band structure for laterally confined Bragg mirrors with circular cross section varying along the longitudinal axis is calculated analytically by means of the coupled-mode theory for structures surrounded laterally either by a metal or by air. Using the scattering state technique, we demonstrate that in porous silicon metallic Bragg reflectors the scattering states form a series of discrete levels with a constant interlevel spacing of about 5 meV, and show that PBO's occur in these structures with a period of about 1 ps at room temperature. PBO's and a PWSL with a comparable period and interlevel spacing are demonstrated in planar multiple-microcavity structures based on III-V semiconductors with cavity length varying along the growth axis. These structures are very promising, since they do not require any lateral confinement, thus avoiding dephasing mechanisms introduced by etching at the lateral sidewalls that can hinder the observation of PBO's.

DOI: 10.1103/PhysRevB.63.035108 PACS number(s): 78.47.+p, 78.66.−w, 78.90.+t

I. INTRODUCTION

Recently electronic Bloch oscillations (EBO's), i.e., oscillations of an electron within the Brillouin zone induced by an applied electric field,[1] have been experimentally demonstrated in semiconductor superlattices.[2,3] An electron in a crystal experiences EBO's if the dephasing time is longer than the oscillation time h/eFd, where e is the electronic charge, F is the applied electric field, and d is the lattice period. On increasing F, the period of the oscillations decreases, thus facilitating the detection of EBO's. However, one cannot apply an arbitrarily intense electric field, since then Zener tunneling between adjacent crystal bands (or superlattice minibands) occurs.[4–7] Up to now EBO's have been observed only in semiconductor superlattices, since these structures exhibit a large supercell in real space, i.e., a large period d, resulting in a small Bloch-oscillation time.

The analogy between an electron in a real crystal and a photon in a dielectric medium[8,9] allows us to speculate on photonic Bloch oscillations (PBO's) in specially designed quasiperiodic dielectric structures. Bloch oscillations are expected to be more easily observed in photonic systems, where dephasing processes play a more minor role than in the electronic case. Recent works[10,11] have addressed the problem of the photonic Wannier-Stark ladder (PWSL) and PBO's. Since the electric field has no effect on photons, one has to envision a different method from that used in the electronic case in order to incline the photonic bands, such as a gradual variation of the elementary cell of the photonic crystal. In this paper we propose two types of photonic structure that seem to be very promising for the experimental detection of PBO's and the PWSL, namely, pillar Bragg mirrors (PBM's) and planar coupled multiple microcavities (MMC's).

The paper is organized as follows. In Sec. II the photonic band structure of PBM's with lateral dimension depending on the longitudinal coordinate is studied analytically by means of the coupled-mode theory. Using the appropriate Maxwell boundary conditions at the boundary between the internal and the external region, both PBM's surrounded laterally by a metal (metallic PBM's) and those surrounded laterally by a dielectric such as air (dielectric PBM's) are analyzed. In Sec. III we focus on PBO's: by means of the scattering state technique, the field intensity is numerically calculated as a function of time and coordinate inside the structure. The numerically obtained period of the PBO's is found to be in excellent agreement with that recovered from the classical formula for Bloch oscillations in electronic crystals. Moreover, by studying the scattering states as a function of energy and coordinate, we show that they form a PWSL with discrete levels having a constant interlevel spacing. Section IV is devoted to planar MMC's with cavity length varying along the growth axis. MMC's act on photons in the same way that superlattices subjected to an electric field act on electrons, since, unlike the previously analyzed PBM's, they are characterized by a discrete spectrum of confined states. PBO's and the PWSL in MMC's are investigated both by means of the scattering state formalism and by a semianalytical approach based on the analogy between electronic and photonic crystals. Section V finally contains concluding remarks. The electric fields and the characteristic equations of cylindrical metallic and dielectric structures are given in the Appendixes.

II. PHOTONIC BAND STRUCTURE IN PILLAR BRAGG MIRRORS

Sections II and III focus on cylindrical dielectric structures periodic along the symmetry axis z surrounded laterally

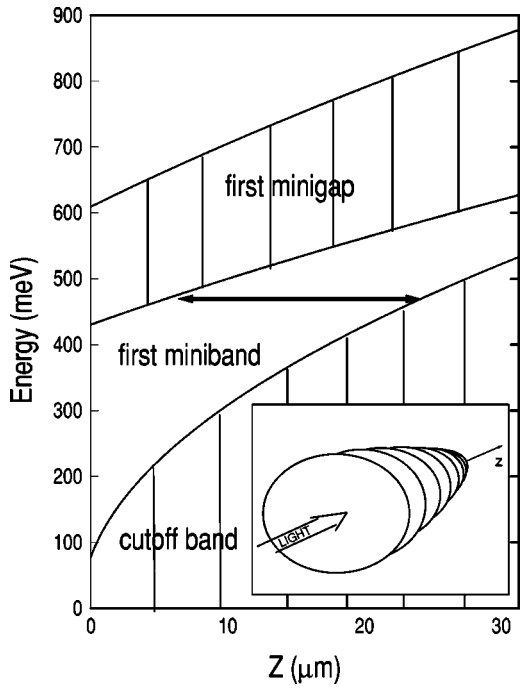

FIG. 1. Photonic band diagram for the TE_{11} mode of the metallic PBM described in the text along the growth direction. The cutoff band, the first allowed miniband, and the first minigap are displayed in the figure. The arrow shows the area where the oscillations are expected to occur for a given light-pulse energy. The inset shows the scheme of the PBM.

either by a metal or by air. The structure (the PBM) is schematically represented in the inset of Fig. 1. The core region is formed by two layers A and B with dielectric constants ε_A and ε_B and thicknesses a and b, respectively, and has a radius $R(z)$ which varies along the symmetry axis. The PBM is surrounded laterally by a ''cladding'' region with the dielectric constant ε_{ext}.

The photonic band structure has been described analytically by means of the coupled-mode theory.[12] Let [in] and [ext] denote the core and the cladding regions. We will denote as the *unperturbed structure* that having the same dielectric constant ε_{ext} as the real (perturbed) structure in [ext] and a dielectric constant that is a weighted average between those of layers A and B in [in], i.e.,

$$\varepsilon_0 = \begin{cases} \dfrac{a\varepsilon_A + b\varepsilon_B}{\Lambda} & [\text{in}], \\ \varepsilon_{\text{ext}} & [\text{ext}], \end{cases} \tag{2.1}$$

where $\Lambda = a + b$. The dielectric constant of the multilayer is then written as the sum of ε_0 and a position-dependent correction $\Delta\varepsilon$,

$$\Delta\varepsilon = \begin{cases} (\varepsilon_B - \varepsilon_A)\dfrac{a}{\Lambda} & [\text{in}], \quad n\Lambda < z < n\Lambda + b \\ -(\varepsilon_B - \varepsilon_A)\dfrac{b}{\Lambda} & [\text{in}], \quad n\Lambda + b < z < (n+1)\Lambda \\ 0 & [\text{ext}], \end{cases} \tag{2.2}$$

where $n = 0,1,2,\ldots$. At the frequency ω the electric field of the structure is the solution in both [in] and [ext] of the wave equation

$$\nabla^2 E + \varepsilon_0 \left(\frac{\omega}{c}\right)^2 E = -\Delta\varepsilon \left(\frac{\omega}{c}\right)^2 E, \tag{2.3}$$

where E is the component of the electric field along one of the three mutually orthogonal axes. Equation (2.3) has been written in a form emphasising that the right-hand side (rhs) represents any deviation of the polarization from that of the unperturbed medium.

We now expand E in terms of the modes of the unperturbed structure at the same ω.

$$E(\rho,z,t) = \frac{e^{-i\omega t}}{2} \sum_\mu e_\mu [A_\mu^{(R)} e^{i\xi_\mu z} + A_\mu^{(L)} e^{-i\xi_\mu z}]. \tag{2.4}$$

The subscript μ is a collective index representing the quantum numbers of the unperturbed modes and their polarization; right- and left-traveling waves along z with z component of the wave vector ξ_μ are denoted with the superscripts (R) and (L), respectively. e_μ is the normalized part of mode μ, which—for fixed lateral dimension—depends only on the transverse coordinates ρ. Variation of the lateral dimension along z makes e_μ also a function of z; this dependence is, however, very small and can safely be neglected.

Inserting Eq. (2.4) in Eq. (2.3) and assuming the adiabatic approximation,[13] namely, that A_μ are slowly varying functions of z, i.e., $|d^2 A_\mu / dz^2| \ll |\xi_\mu dA_\mu / dz|$, we obtain

$$\sum_\mu 2i\xi_\mu e_\mu \left(\frac{dA_\mu^{(R)}}{dz} e^{i\xi_\mu z} - \frac{dA_\mu^{(L)}}{dz} e^{-i\xi_\mu z}\right) = -\Delta\varepsilon \left(\frac{\omega}{c}\right)^2 \sum_\mu e_\mu (A_\mu^{(R)} e^{i\xi_\mu z} + A_\mu^{(L)} e^{-i\xi_\mu z}). \tag{2.5}$$

Equation (2.5) is easily derived if one recalls that e_μ satisfies the wave equation

$$\left[\nabla_T^2 + \left(\varepsilon_0 \frac{\omega^2}{c^2} - \xi_\mu^2\right)\right] e_\mu = 0 \tag{2.6}$$

(∇_T^2 is the transverse Laplacian operator). Taking the scalar product with e_ν and integrating in the plane, the following equation is obtained:

$$\left(\frac{dA_\nu^{(R)}}{dz} e^{i\xi_\nu z} - \frac{dA_\nu^{(L)}}{dz} e^{-i\xi_\nu z}\right) = \sum_{m=-\infty}^{+\infty} \sum_\mu \kappa_{\mu\nu m} (A_\mu^{(R)} e^{i[\xi_\mu + (2\pi/\Lambda)m]z} + A_\mu^{(L)} e^{-i[\xi_\mu - (2\pi/\Lambda)m]z}), \tag{2.7}$$

$$\kappa =: \kappa_{\mu\nu m} = i\left(\frac{\omega}{c}\right)^2 \frac{b_m}{2\xi_\nu} (\varepsilon_B - \varepsilon_A) \langle e_\nu | e_\mu \rangle_{\text{in}},$$

where $\langle e_\nu | e_\mu \rangle_{\text{in}}$ indicates that the integral between e_ν and e_μ is restricted to the internal region only. In deriving Eq. (2.7), $\Delta\varepsilon$ has been represented as the Fourier series

$$\Delta\varepsilon(\omega,\rho,z)=\begin{cases}(\varepsilon_B-\varepsilon_A)\displaystyle\sum_{m=-\infty}^{m=+\infty} b_m \exp\left(i\frac{2\pi}{\Lambda}mz\right) & [\text{in}]\\ 0 \quad [\text{out}]\end{cases} \tag{2.8}$$

with

$$b_m=\begin{cases}\dfrac{1}{\pi m}\exp\left(-i\dfrac{\pi}{\Lambda}mb\right)\sin\left(\dfrac{\pi}{\Lambda}mb\right), & m\neq 0\\ 0 \quad m=0\end{cases}. \tag{2.9}$$

The rhs in Eq. (2.7) may be interpreted as a source wave term driving the right- and left-traveling waves. In order for a wave to be driven by a source, the source and the wave need to have nearly the same phase dependence so that the interaction does not average to zero with distance of propagation z. Keeping only the resonant terms in Eq. (2.7) two coupled equations for the coefficients $A_\nu^{(R)}$ and $A_\nu^{(L)}$ are finally obtained. In the following we will consider the case in which the dielectric perturbation couples strongly only left- and right- traveling waves with the same quantum numbers. The coupled equations then reduce to

$$\frac{dA_\nu^{(R)}}{dz}=\kappa A_\nu^{(L)}\exp(-2i\Delta\xi z),$$

$$\frac{dA_\nu^{(L)}}{dz}=\kappa^* A_\nu^{(R)}\exp(2i\Delta\xi z), \tag{2.10}$$

where the symbols $\Delta\xi =: \Delta\xi_{\nu m}=\xi_\nu-(\pi/\Lambda)m$ and $\kappa =: \kappa_{\nu\nu m}$ have been introduced for notational convenience. The solutions of Eq. (2.10) for $A_\nu^{(R)}$ and $A_\nu^{(L)}$ (see Ref. 12) show that—whenever $|\kappa|>\Delta\xi$—the propagation wave vector of the mode acquires an imaginary part which is responsible for the exponential decay of the power along the perturbed region; the corresponding energy window constitutes the mth stop band for mode ν.

We now apply this theory to multilayer structures with a circular cross section surrounded laterally by a metal and by air.

A. Multilayer surrounded laterally by a metal

The unperturbed modes together with their characteristic equations are given in Appendix A. These modes, which are found by solving Maxwell equations in the internal region and by imposing Maxwell boundary conditions at the metallic interface, belong to two distinct classes: the TE modes, with vanishing longitudinal component of the electric field, and the TM modes, with vanishing longitudinal component of the magnetic field.[14]

Since $\Delta\varepsilon$ is a scalar, the dielectric perturbation couples only TE to TE and TM to TM modes, but not TE to TM modes. Moreover, $\langle e_\mu | e_\nu \rangle_{\text{in}}=\delta_{\mu\nu}$, since the modes are perfectly confined in the internal region; thus $\Delta\varepsilon$ couples only right- and left-traveling waves with the same quantum numbers, as can be seen from Eq. (2.7).

For notational convenience, in the following we will omit the index ν with the understanding that we are dealing with a well-specified mode and polarization (TE or TM). At a given radius, a mode can propagate within the structure only when (a) ω is beyond the *cutoff frequency* $\omega_0^{(\text{top})}=c\beta/\sqrt{\varepsilon_0}$, and (b) ω does not fall inside a stop band. β is the transverse component of the wave vector, depending on the radius and on the quantum numbers of the mode. It is determined using Eqs. (A2) and (A4) for TM and TE modes, respectively, and it is connected with ω and with the longitudinal component of the wave vector ξ through the relation $\beta=\sqrt{\varepsilon_0(\omega/c)^2-\xi^2}$.

The first allowed photonic band lies between the cutoff frequency $\omega_0^{(\text{top})}$ and the bottom of the first stop band, whereas the frequencies of the $(m+1)$th allowed miniband with $m\geqslant 1$ lie between the top of the mth ($\omega_m^{(\text{top})}$) and the bottom of the $(m+1)$th ($\omega_{m+1}^{(\text{bot})}$) stop bands. For $m\geqslant 1$, $\omega_m^{(\text{top})}$ and $\omega_{m+1}^{(\text{bot})}$ are calculated as follows. (1) The coupled-mode theory gives $\xi_m^{(\text{top})}=m\pi/\Lambda+|\kappa_m|$ at the top of the mth stop band, which corresponds to the frequency

$$\omega_m^{(\text{top})}=\frac{c}{\sqrt{\varepsilon_0}}\sqrt{(m\pi/\Lambda+|\kappa_m|)^2+\beta^2}. \tag{2.11}$$

(2) At the bottom of the $(m+1)$th stop band $\xi_m^{(\text{bot})}=(m+1)\pi/\Lambda-|\kappa_{m+1}|$, corresponding to the frequency

$$\omega_{m+1}^{(\text{bot})}=\frac{c}{\sqrt{\varepsilon_0}}\sqrt{[(m+1)\pi/\Lambda-|\kappa_{m+1}|]^2+\beta^2}. \tag{2.12}$$

$|\kappa_j|$ is given by

$$|\kappa_j|=\left(\frac{\omega_j}{c}\right)^2\frac{b_j}{2}\frac{|(\varepsilon_B-\varepsilon_A)|}{(j\pi/\Lambda)},$$

with $\omega_j=(c/\sqrt{\varepsilon_0})\sqrt{(j\pi/\Lambda)^2+\beta^2}$ $(j=m,m+1)$ representing the center of the jth stop band. We note that the whole dependence of the stop-band edge on the radius is contained in the transverse component of the wave vector β.

The width of the $(m+1)$th allowed miniband is finally calculated as

$$\Delta_{m+1}=[\omega_{m+1}^{(\text{bot})}-\omega_m^{(\text{top})}] \quad (m\geqslant 0). \tag{2.13}$$

In Fig. 1 we show the first allowed photonic miniband for the fundamental TE_{11} mode of a metallic PBM surrounded laterally by a metal. Solving Eq. (A4) we obtain $\beta(z)=1.841/R(z)$. The analyzed structure is formed by 46 periods of alternating porous silicon layers with refractive indices $n_a=\sqrt{\varepsilon_a}=1.27$ and $n_b=\sqrt{\varepsilon_b}=2.25$ and layer thicknesses $a=380$ and $b=300$ nm, respectively. Thus the total thickness of the PBM is $L=31.28\,\mu$m. We assume that the radius varies along the symmetry axis as

$$R(z)=\frac{\theta}{\sqrt{Q+z}}. \tag{2.14}$$

The selected constants $Q=680$ nm and $\theta=6.87\times10^4$ nm$^{3/2}$ yield radii $R=2.63$ and 0.384 μm at the beginning ($z=0$) and end ($z=L$) of the PBM. Porous silicon seems to be a very promising material for the experimental detection of PBO's because it allows altering the refractive index in a wide range. The technology of growth of Bragg mirrors from porous silicon is quite well developed, and its chemical etching and metallization have become quite ordinary operations.[15]

The varying lateral confinement for the photon, which is provided by the variation of the radius of the PBM along *z*, gives rise to the inclined minibands of Fig. 1 and plays the same role as an electric field applied along the growth direction in a conventional superlattice. Note, however, that the inclination angle is different for different miniband edges, unlike the case of a conventional superlattice in an electric field. Strictly speaking, the oscillations of light within such an inclined miniband are not true Bloch oscillations, since the system under study is not periodic. That is why tunneling of confined light modes between two spatially separated minibands (Zener tunneling) is possible in the present case, as will be seen from the calculations below. The arrow in Fig. 1 shows the region where PBO's are expected to occur when a pulse centered at the same frequency as the ordinate in the plot impinges on the sample. Note that the photonic localization area within the structure can be tuned simply by changing the energy of the incident pulse: this feature does not characterize light oscillation within a conventional Fabry-Pérot resonator.

The analogy with the electronic case suggests introducing an effective field *F* acting on the photon. This is not a simple task; in fact, if the variation of the band edges were a linear function of *z*, then a constant effective electric field could be extracted from the inclination angle of the miniband of the PBM. However, only the top of the allowed miniband has a linear variation with *z* in the whole PBM, whereas the bottom edge varies linearly only for large *z*, as can be seen in Fig. 1. All the same, we can give a rough estimate by considering the region with $z\geqslant15$ μm and defining the effective field as the average of those extracted from the inclination angles of the top and bottom edges of the miniband. This gives $F=7.8\times10^3$ V/m. Further stressing the analogy with the electronic case, using the classical formula

$$\tau_B=h/eF\Lambda \tag{2.15}$$

we can also estimate that PBO's occur with a period $\tau_B=0.78$ ps. The detailed numerical analysis of PBO's in Sec. III shows that this rough estimate is really in very good agreement with the exact numerical result.

B. Multilayer surrounded laterally by air

The propagating modes of a dielectric with circular cross section surrounded laterally by air are conventionally called HF and EH modes.[14] Their characteristic equations together with their approximate expressions obtained by keeping only the dominant circular component are given in Appendix B.

The dielectric perturbation couples only HE to HE and EH to EH modes in this case also. Moreover, the structure has cylindrical symmetry around the *z* axis, which leads to coupling between modes with the same azimuthal quantum number *l* only. However, the lack of translational invariance in the plane is responsible for coupling between modes with different radial numbers *n*. As already stated, we here examine the situation in which the dielectric perturbation couples only right- and left-traveling waves with the same quantum numbers.

The center and width of the $(m+1)$th allowed photonic band can be expressed in the same way as in Sec. II A. However, the transverse wave vector now depends on the longitudinal wave vector through the characteristic equation (B4), which uniquely determines β and ω once ξ is specified. Moreover, κ_m now also has a small dependence on the radius. In fact, the modes can now leak into the air, which implies that $|\langle e_\mu|e_\nu\rangle_{\text{in}}|<1$. The degree of leakage is a function of the radius and varies along the structure, being negligible at large radii where the modes are well confined in the internal region, and becoming sizable at small radii. However, in this case also the strongest dependence of the band energy on the radius comes from the variation of β with *R*.

III. BLOCH OSCILLATIONS AND WANNIER-STARK LADDER IN PILLAR BRAGG MIRRORS

The electric field created in the system by an incident pulse of spectral function $g(\omega)$ is calculated by means of the scattering state method.[11,16] By this formalism the time-and coordinate-dependent electric field within the structure can be found as follows:

$$E_g(z,t)=\frac{1}{2\pi}\int_{-\infty}^{+\infty}E_g(\omega,z)\exp(-i\omega t)d\omega \tag{3.1}$$

where

$$\tilde{E}_g(\omega,z)=\tilde{E}(\omega,z)g(\omega). \tag{3.2}$$

$\tilde{E}(\omega,z)$ are the scattering states of the system, namely, the solutions of the stationary Maxwell equations; they are obtained by the transfer matrix method. The allowed miniband energies are given by the condition (which is a consequence of the Bloch theorem)

$$-1\leqslant(a_{11}+a_{22})/2\leqslant1, \tag{3.3}$$

where a_{11} and a_{22} are the diagonal elements of the transfer matrix across the period of the structure. Note that the formulas (2.13) and (2.3) formally yield the same band structure, but the condition (2.3) has a more general character and applies also to the multiple-microcavity structures discussed in Sec. IV.

Depending on the characteristic equation used in determining the transverse wave vector β, both metallic and dielectric PBM's can be analyzed. Here we will focus only on the behavior of the fundamental TE_{11} mode in a metallic PBM described by the same parameters as in Sec. II A. Moreover, we consider an incident pulse having the spectral function

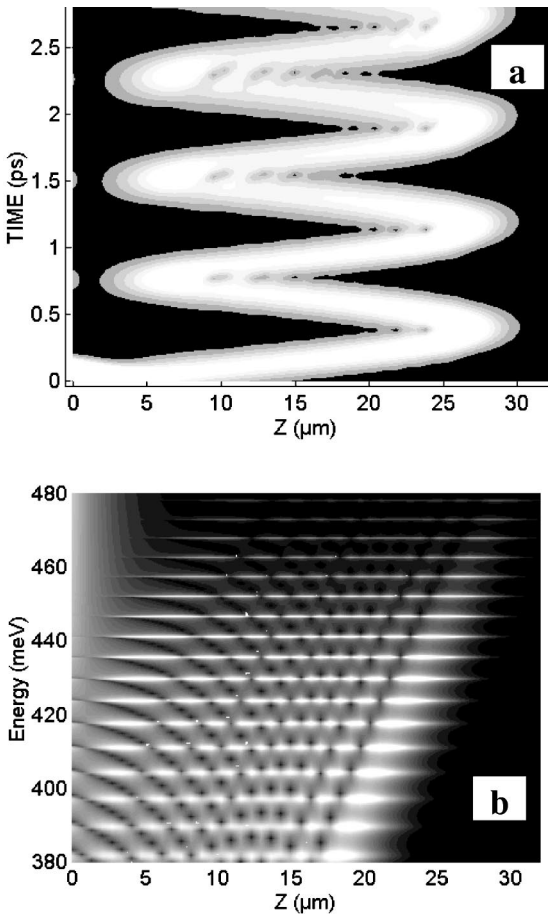

FIG. 2. (a) Propagation of a Gaussian pulse of light in the PBM described in the text. The brightness is proportional to the intensity of the electric field. (b) Coordinate- and energy-dependent electric field induced by an infinitely short light pulse in the PBM (scattering states of the PBM). The brightness is proportional to the intensity of the electric field.

$$g(\omega)=\frac{\hbar}{\sqrt{\pi}\delta}\exp\left[-\left(\frac{\hbar\omega-E_0}{\delta}\right)^2\right], \tag{3.4}$$

with $E_0=500\,\mathrm{meV}$ and $\delta=45\,\mathrm{meV}$.

Figure 2(a) shows the calculated electric field induced in the structure by the incident pulse (3.4) as a function of the time and of the coordinate along the growth direction. The brightness in the figure is proportional to the electric field intensity. One can see an initial decrease of the intensity when the pulse tunnels through the minigap region $0<z<6\,\mu$m; oscillations then occur approximately between $z=4$ and 30 μm. Indeed, these are the Bloch oscillations of the light within the inclined miniband. Note that the inclined minigap at the beginning of the structure acts as a filter, selecting only the low-frequency wing of the pulse. The period of the PBO's calculated from Fig. 2(a) is $\tau_B=0.77\,\mathrm{ps}$, in excellent agreement with the classical estimate of Sec. II.

Figure 2(b) shows the scattering states of the PBM. One can observe a series of discrete states. They are broad and irregularly spaced at low energies since they overlap with the continuum in this case. Then, at higher energies, these states become totally confined within the structure. They have a sharply defined energy and, moreover, are regularly spaced. Visibly, they form the frequency counterpart of the PBO's, namely, the PWSL. The interlevel spacing between these states is $\Delta=5.3\,\mathrm{meV}$, which corresponds exactly to that derived from the period of the PBO's, $\Delta=h/\tau_B$.

Experimentally, it can be hard to detect PBO's in time-resolved reflection spectra. In fact, PBO's compete with dephasing processes; for this reason the lateral profile of the PBM has to be precisely controlled, a task that can be difficult with state-of-the-art etching techniques. In the next section we present an alternative structure that is free of these disadvantages and could thus be more suitable for the observation of PBO's.

IV. PHOTONIC BLOCH OSCILLATIONS IN COUPLED MULTIPLE MICROCAVITIES

The appearance of semiconductor superlattices was a key step toward the observation of EBO's. The artificial band structure containing minibands of a few hundreds of meV was much more suitable for EBO's than that of bulk semiconductors. The laterally confined Bragg mirrors analyzed in the previous sections can be formally considered as optical superlattices. The layers of the lower-index material play the role of quantum wells (QW's), and the layers with the higher index are the equivalent of the barriers in a conventional superlattice. It is essential to note here, however, that the photonic confinement along the axis of the structure is possible only because of the lateral confinement of light. In periodic planar multilayer structures the interfaces are semitransparent for light and, at variance with the electronic levels in QW's, discrete confined photonic levels are not formed.

Thus, even though the Bragg mirrors exhibit stop bands similar to the minigaps of electronic superlattices, this similarity is not complete. In fact, the real optical equivalents of QW's are microcavities, since they are characterized by a discrete spectrum of confined states. Recently, coupled microcavity structures have been investigated theoretically and experimentally.[17] The optical coupling lifts the degeneracy between the optical modes in identical cavities. In the limit of an infinite multiple-microcavity structure, optical bands develop that are completely analogous to the minibands in semiconductor superlattices.

In order to obtain PBO's, one has to envision a way to incline the optical band. The easiest way to do this with MMC's is to slightly increase (or decrease) the cavity width from the beginning to the end of the structure.

This section is devoted to the analysis of MMC's formed by cavities with varying thicknesses, which are expected to exhibit PBO's. An advantage of such structures with respect to the previously discussed PBM's is that they do not require any lateral confinement and can be grown by the usual epitaxial techniques like metal-organic chemical vapor deposition or molecular beam epitaxy without further etching.

Our model structure is schematically depicted in Fig. 3. It is formed by N λ cavities of refractive index n_a labeled $M_1, M_2, \ldots, M_N$. In the absence of coupling, the energy of

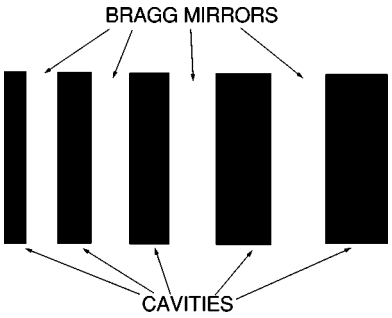

FIG. 3. Scheme of the multiple-microcavity structure with the cavity width varying along the structure axis.

the fundamental mode of the ith cavity is E_i, corresponding to a wavelength in the vacuum of $\lambda_i = hc/E_i$. Each cavity is surrounded by two distributed Bragg mirrors (DBR's) formed by k layers of index n_a (high-index material) and $(k+1)$ layers of index n_b (low-index material; $n_b < n_a$). Thus each elementary cell of our optical superlattice consists of one DBR containing $k+\frac{1}{2}$ pairs of dielectric layers and of a λ cavity, and has the length

$$d_i = \lambda_i \left(\frac{k/4+1}{n_a} + \frac{k/4+1/4}{n_b} \right). \tag{4.1}$$

Stressing the analogy with the electronic case discussed in Sec. II, we define an effective local electric field in each cavity as

$$F_i = \frac{E_i - E_{i-1}}{e d_i}. \tag{4.2}$$

Moreover, the eigenmode of the ith cavity can be interpreted as the ith step of the PWSL. In order to obtain PBO's, the spacing Δ between the steps of the PWSL must be constant; this implies that $eF_i d_i = -\Delta$ for any $i = 1,2,...,N$, or, equivalently,

$$\frac{1}{\lambda_i} - \frac{1}{\lambda_{i-1}} = -\frac{\Delta}{hc}. \tag{4.3}$$

If the condition $E_i \gg \Delta$ is met, the last equation can be approximately rewritten as

$$\lambda_i = \lambda_1 \left[1 + \frac{i-1}{c\tau_B} \lambda_1 + (i-3)(i-2) \left(\frac{\lambda_1}{c\tau_b} \right)^2 \right], \tag{4.4}$$

where $\tau_B = h/\Delta$ is the period of the PBO's.

The spatial extension of the oscillations is

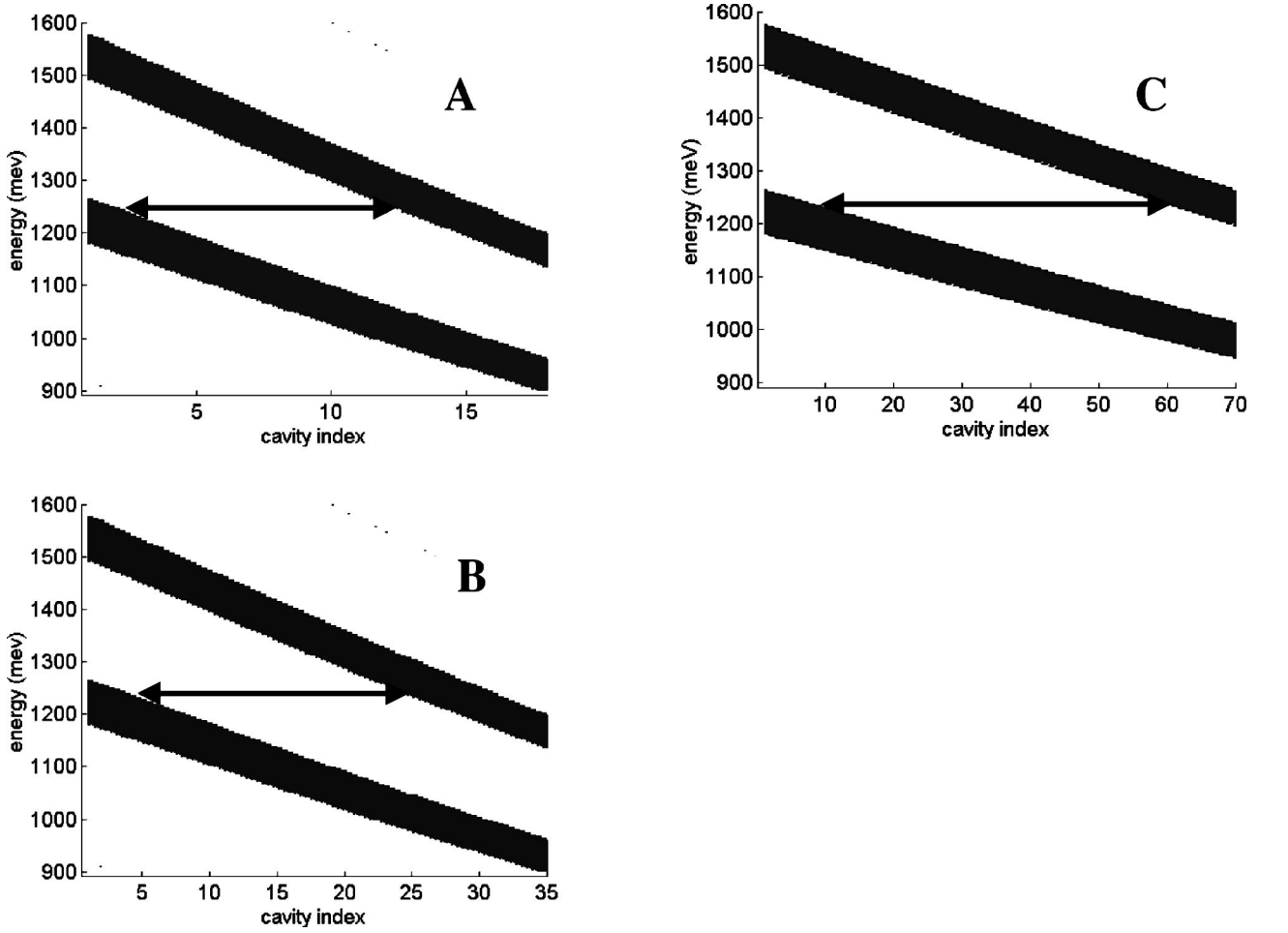

FIG. 4. Photonic band diagram of the *A*, *B*, and *C* MMC's along the growth direction. White regions represent the minibands, dark regions represent the minigaps.

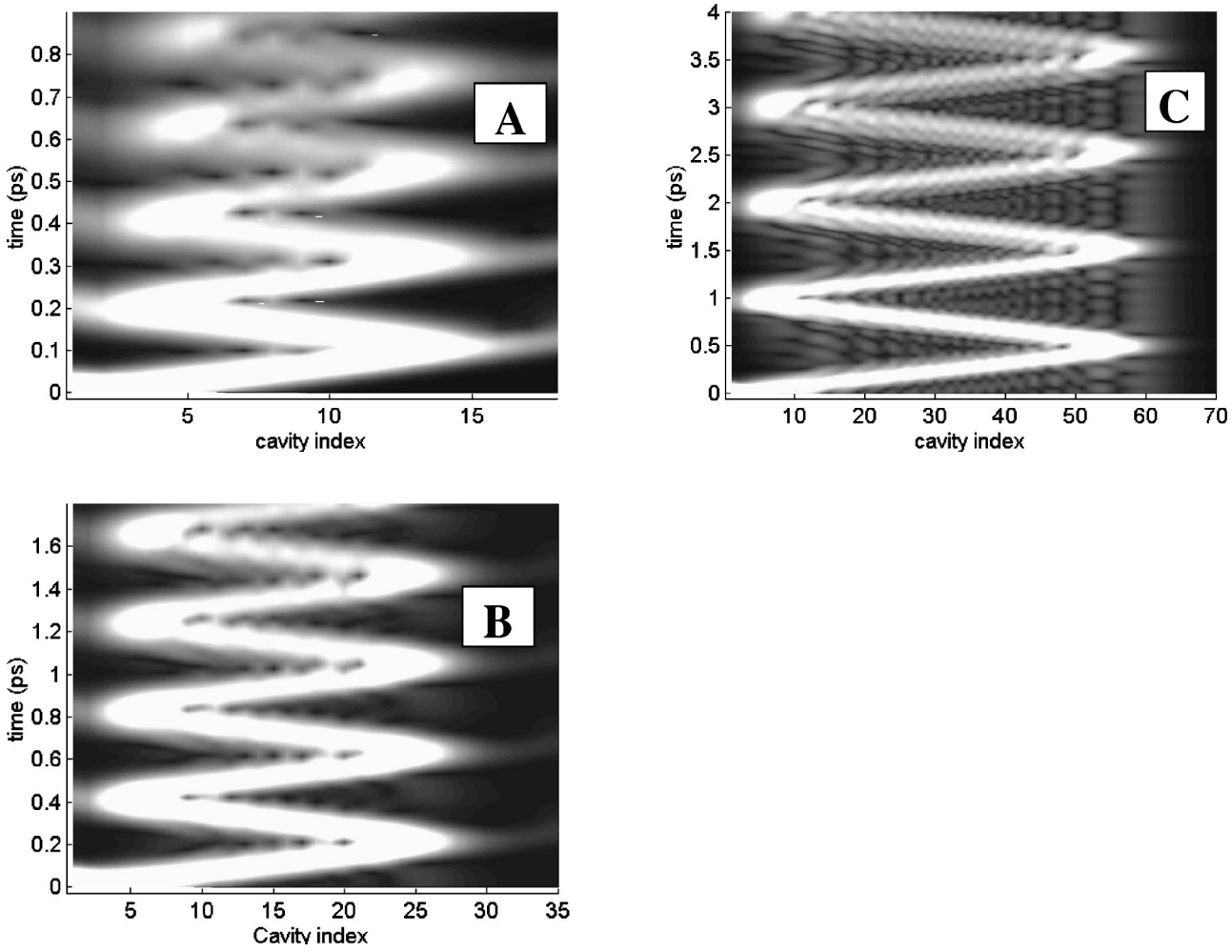

FIG. 5. Propagation of a Gaussian pulse of light in the MMC's labeled *A*, *B*, and *C*. The brightness is proportional to the intensity of the electric field.

$$D \equiv v_{\mathrm{av}} \frac{\tau_B}{2} = \frac{(k/4+1)/n_a^2 + (k/4+1/4)/n_b^2}{(k/4+1)/n_a + (k/4+1/4)/n_b}.$$

v_{av} is the weighted averaged velocity of the light propagating in homogeneous media with the same refractive indices as the layers forming the MMC. In order for PBO's to occur, the extension D cannot exceed the total length of the structure; thus

$$D < \sum_{i=1}^{N} d_i . \tag{4.5}$$

In III-V semiconductor microcavities the dielectric contrast is small, in general, i.e., $n_A - n_B < n_A, n_B$; if, in addition, the variation of the width of the cavity layers along the structure is smaller than λ_1, we can approximately estimate the total number of periods required to observe PBO's using the condition [derived from Eqs. (4.4) and (4.5)]

$$\frac{c\tau_B}{2\lambda_1} < N(k/2+5/4). \tag{4.6}$$

We then see that, by simply adjusting the oscillation period (i.e., the energy difference between the cavity modes) and the central wavelength, an optical superlattice sustaining PBO's is obtained.

In the electronic case the extension D of the oscillation is related to the width W of the superlattice miniband by the relation

$$D = W/eF \tag{4.7}$$

(F is an external electric field). In our case, this formula can be rewritten as

$$W = e\sum_{i=p}^{q} F_i d_i = (q-p)\Delta, \tag{4.8}$$

where p and q satisfy the relation

$$D = \sum_{i=p}^{q} d_i . \tag{4.9}$$

An estimate for the difference $p-q$ can be found from Eq. (4.6) as

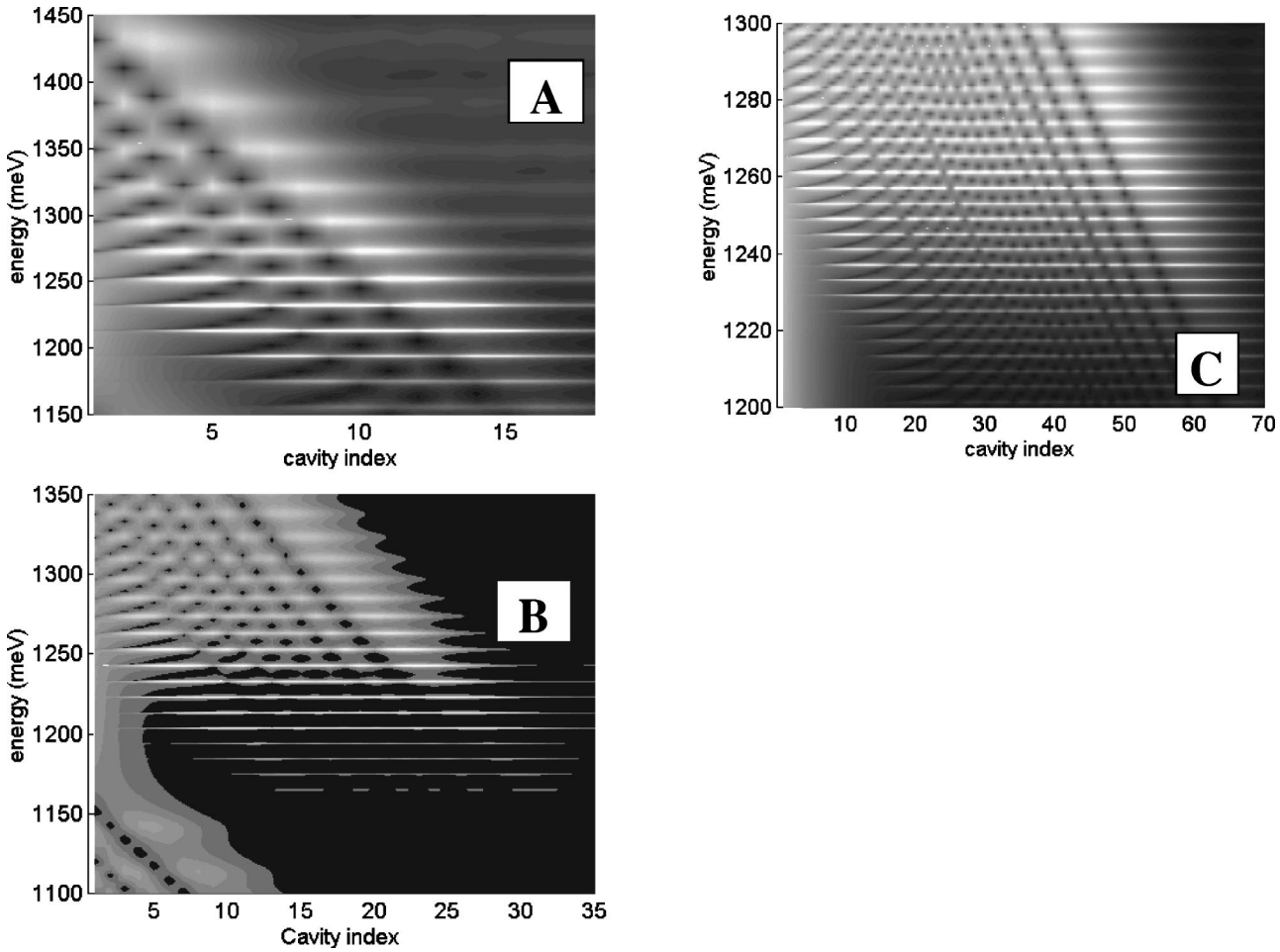

FIG. 6. Coordinate- and frequency-dependent electric field induced by an infinitely short light pulse in the MMC's labeled *A*, *B*, and *C*. The brightness is proportional to the intensity of the electric field.

$$p-q=\frac{c\tau_B}{2\lambda_1(k/2+5/4)}. \tag{4.10}$$

The corresponding bandwidth is

$$W=\frac{c\tau_B\Delta}{2\lambda_1(k/2+5/4)}=\frac{hc}{2\lambda_1(k/2+5/4)}. \tag{4.11}$$

Figure 4 represents the calculated band structure for three GaAs/AlAs samples (labeled *A*, *B*, and *C*), all with the same central width $\lambda_1=0.9\,\mu$m, but formed by a different number *N* of cavities. Parameters have been chosen in order to produce PBO's with periods of 0.2, 0.4, and 1 ps, respectively. Since for observation of the PBO's the condition (4.6) must be satisfied, we chose $k=2$ for the three samples and $N_A=18$, $N_B=35$, and $N_C=70$ for samples *A*, *B*, and *C* respectively. Finally, the thicknesses of the different slabs were chosen according to Eq. (4.1). The band structure was calculated by means of the transfer matrix approach and using Eq. (3.3). The inclined minigaps (black) and minibands (white) in Fig. 4 clearly show that the factor $F_i d_i$ is a constant over the whole structure, which implies that the band edges depend linearly on the cavity number index *i*. The numerically obtained bandwidth is about 250 meV. This is in good agreement with the 300 meV width obtained from the approximate analytical relation (4.11). By illuminating the samples with a pulse centered just below the lower limit of the miniband, namely, at 1250 meV, PBO's can be created. The arrows show the spatial and spectral region where the oscillations should take place. On longer structures, it is in principle possible to tune the area where the oscillations are localized by changing the energy of the incident pulse, as already described in Sec. II.

Figure 5 shows the electric field created by a Gaussian pulse of light as a function of the time and of the cavity number index for the three samples of Fig. 4. The incident pulse is centered at 1250 meV, which is far enough inside the GaAs gap and in the classical work area of Ti:sapphire lasers; its time duration is 50, 100, and 200 fs for samples *A*, *B*, and *C*, respectively. The calculation was performed by means of the scattering state technique for planar heterostructures. The brightness in the figure is proportional to the electric field intensity. One can see that the pulses entering the structures at $t=0$ and $z=0$ first pass through the minigap regions where they lose intensity, and then start to oscillate within the minibands with periods of 0.2, 0.4, and 1 ps, for samples *A*, *B*, and *C* respectively.

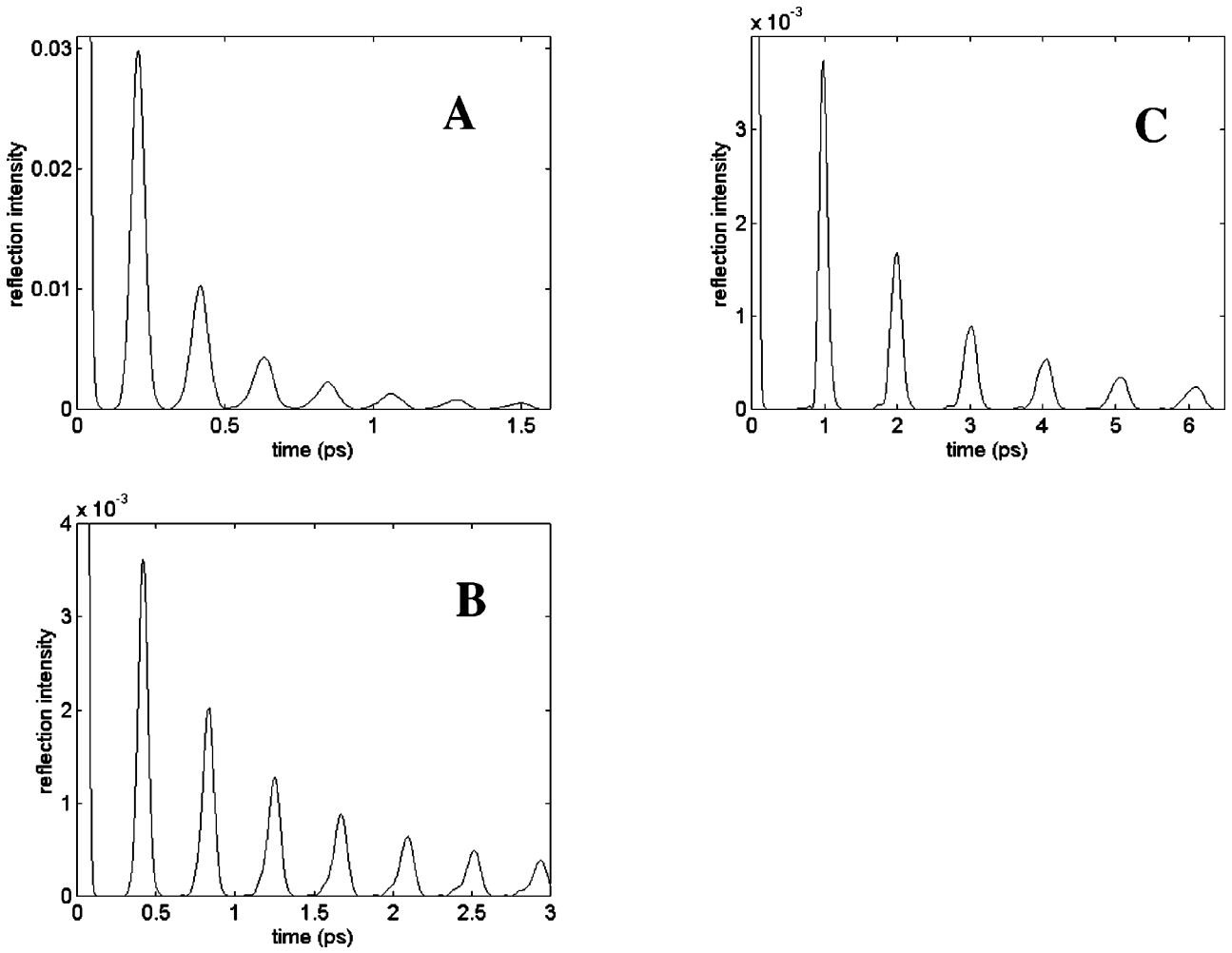

FIG. 7. Calculated time-resolved reflection spectra of the three MMC's labeled *A, B,* and *C* excited by the same light pulse as in Fig. 5.

Figure 6 represents the energy of the scattering states for the three structures as a function of the cavity index number. They are very well resolved (particularly in the case of fully confined states, i.e., for energies below 1250 meV) and regularly spaced with an interlevel spacing Δ of 20.5, 10.25, and 4.1 meV for the three samples. The excellent agreement with the value estimated from Eqs. (4.3) and (4.4) supports the interpretation of the scattering state levels as steps of the PWSL.

The most efficient way to observe PBO's experimentally is to measure the time-resolved reflection. Figure 7 shows the calculated time-resolved reflection spectra for the three samples described above. The plotted intensity has been normalized in the figure. In the three cases, the reflection exhibits very well-defined oscillations with periods equal to those of the PBO's. Moreover, the reflected intensity is quite high, suggesting that oscillations are relatively easily detected in time-resolved reflection experiments. Structure *B* seems to be the most suited for experimental realization, since it is much thinner than structure *C* and thus does not require an extremely long growth time. On the other hand, PBO's occur with a period that is two times longer than in structure *A*, which is expected to provide easier detection.

V. CONCLUSIONS

The aim of this paper was to show that the analogy between electronic and photonic crystals goes beyond the band structure similarity. The electronic and photonic transport properties are also subject to the same rules, in general. In particular, this analogy manifests itself in the phenomenon of Bloch oscillations. PBO's can be more easily observed, in general, than EBO's, since the coherence length of light much exceeds the electronic coherence length. On the other hand, the observation of PBO's requires great effort in structure preparation. The role of the electric field for photons is played by a gradual variation of the crystal cell that causes the gradual variation of the band edge energies. In this work we have analyzed two possible designs of photonic structure appropriate for observation of PBO's. Variation of the lateral dimension of the unit cell provides the necessary gradient of the band edges in the first case (PBM's), whereas, in the second case (MMC's), the same goal is achieved by changing the unit cell dimension in the light propagation direction.

At the present stage of epitaxial growth technology, the second model seems to be more easily realizable, since it does not require any lateral etching. The advantage of the first model is that it does not require a precise control of the

layer thicknesses during growth. Moreover, pillar structures are now routinely fabricated,[18,19] thus making the detection of PBO's in PBM's a feasible technological challenge.

Detection of PBO's requires time-resolved optical experiments with a femtosecond resolution, which is the state of the art of modern coherent linear optics. We realize that in any case fabrication of appropriate structures and experimental observation of the PBO's still is a question of substantial effort. What could be the possible technological output of the PBO's physics? In our opinion, generation of a terahertz modulated optical signal at room temperature and in a wide frequency range is an attractive perspective that emerges directly from the proposed optical experiments.

ACKNOWLEDGMENT

We acknowledge partial support from the EU ''Clermont'' program, Contract No. HPRN-CT-1999-00132.

APPENDIX A

Fields in cylindrical structures are conveniently described using the cylindrical coordinate system (ρ,ϕ,z). A structure of radius R and dielectric constant ε_0 surrounded laterally by a metal sustains TM and TE modes, characterized by an azimuthal quantum number l ($l=0,\pm1,\pm2,...$) and by a radial quantum number n ($n=1,2,3,...$). For TM modes they are given by

$$\left.\begin{aligned} E_\rho &= \mp iA_{ln}\frac{\xi_{ln}}{\beta_{ln}}I_l'(\beta_{ln}\rho)\\ E_\phi &= \pm A_{ln}\frac{\xi_{ln}l}{\beta_{ln}^2\rho}I_l(\beta_{ln}\rho)\\ E_z &= A_{ln}I_l(\beta_{ln}\rho)\end{aligned}\right\}\times e^{il\phi}e^{i\xi_{ln}z}e^{-i\omega t} \qquad \text{(A1)}$$

(I_l is a Bessel function of the first type of order l and A_{ln} is the normalization factor). The characteristic equation for TM modes

$$I_l(\beta_{ln}R)=0 \qquad \text{(A2)}$$

is obtained by requiring that the longitudinal component of the electric field vanishes at the air/metal interface. This equation gives the transverse component of the wave vector for mode (ln) as $\beta_{ln}=x_{ln}/R$ (x_{ln} is the nth root of the Bessel function of order l).

For TE modes,

$$\left.\begin{aligned} E_\rho &= A_{ln}\frac{\omega l}{c\beta_{ln}^2\rho}I_l(\beta_{ln}\rho)\\ E_\phi &= iA_{ln}\frac{\omega}{\beta_{ln}c}I_l'(\beta_{ln}\rho)\\ E_z &= 0\end{aligned}\right\}\times e^{il\phi}e^{i\xi_{ln}z}e^{-i\omega t}. \qquad \text{(A3)}$$

The characteristic equation for TE modes is

$$I_l^{IH}(\beta_{ln}R)=0. \qquad \text{(A4)}$$

The TE_{11} is the lowest-order mode that can propagate in the structure.

APPENDIX B

Solution of the Maxwell equations in the internal and in the external region (air) with the requirement that the longitudinal components of the electric and magnetic fields are continuous at the interface provides two classes of solutions, denoted as HE and EH modes, which are characterized by the azimuthal quantum number l and the radial quantum number n. For these modes the three linearly polarized components of the electric and magnetic fields are in general all nonvanishing. In order to circumvent this difficulty it is convenient to write the fields in terms of their circular components; noting that either the positive or the negative circular component dominates the in-plane intensity distribution and is much larger also than the longitudinal one, we approximate the modes by keeping only this Stark component. Only for EH_{0n} and HE_{0n} modes do the two circular components have the same weight and the modes exhibit pure TE and TM character, respectively. The approximate expressions for the fields in the internal region are (upper sign for the EH modes; lower sign for the HE modes)

$$\left.\begin{aligned} l\geqslant 1, &\quad E\approx\frac{1}{N_{ln}}I_{l\pm1}(\beta_{ln}\rho)\frac{1}{\sqrt{2\pi}}e^{i(l\pm1)\phi}\hat{u}_\mp\\ l\leqslant -1, &\quad E\approx\frac{1}{N_{ln}}I_{|l|\pm1}(\beta_{ln}\rho)\frac{1}{\sqrt{2\pi}}e^{-i(|l|\pm1)\phi}\hat{u}_\pm\\ l=0, &\quad E\approx\frac{1}{\sqrt{2\pi}}\frac{1}{N_{0n}}I_1(\beta_{0n}\rho)\begin{pmatrix}\hat{\Phi}\\ \hat{\rho}\end{pmatrix}\end{aligned}\right\}\times e^{i\xi_{ln}z}e^{-i\omega t}. \qquad \text{(B1)}$$

In the external region,

$$\left.\begin{aligned} l\geqslant 1, \quad & E\approx \mp\frac{1}{N_{ln}}\left(\frac{\beta_{ln}}{q_{ln}}\frac{I_l(\beta_{ln}R)}{K_l(q_{ln}R)}\right)K_{l\pm1}(q_{ln}\rho)\frac{1}{\sqrt{2\pi}}e^{i(l\pm1)\phi}\hat{u}_{\mp} \\ l\leqslant -1, \quad & E\approx \mp\frac{1}{N_{ln}}\left(\frac{\beta_{ln}}{q_{ln}}\frac{I_{|l|}(\beta_{ln}R)}{K_{|l|}(q_{ln}R)}\right)K_{|l|\pm1}(q_{ln}\rho)\frac{1}{\sqrt{2\pi}}e^{-i(|l|\pm1)\phi}\hat{u}_{\pm} \\ l=0, \quad & E\approx -\frac{1}{\sqrt{2\pi}}\frac{1}{N_{0n}}\left(\frac{\beta_{0n}}{q_{0n}}\frac{I_0(\beta_{0n}R)}{K_0(q_{0n}R)}\right)K_1(q_{0n}\rho)\begin{pmatrix}\hat{\Phi}\\ \hat{\rho}\end{pmatrix} \end{aligned}\right\}\times e^{i\xi_{ln}z}e^{-i\omega t}. \tag{B2}$$

I_l (K_l) are the modified Bessel functions of the first type of order l; $\beta_{ln}=\sqrt{\varepsilon_0(\omega/c)^2-\xi_{ln}^2}$; $q_{ln}=\sqrt{\xi_{ln}^2-(\omega/c)^2}$; $\hat{u}_{\pm}$ are rotating unit vectors, which are expressed in terms of the Cartesian $(\hat{x},\hat{y})$ and polar $(\hat{\rho},\hat{\Phi})$ unit vectors as $\hat{u}_{\pm}=(1/\sqrt{2})(\hat{x}\pm i\hat{y})=(1/\sqrt{2})(\hat{\rho}\pm i\hat{\phi})e^{\pm i\phi}$. N_{ln} is the normalization factor, which is given by

$$N_{ln}=\left[\int_0^R d\rho\,\rho I_{|l|\pm1}^2(\beta_{ln}\rho)+\left(\frac{\beta_{ln}}{q_{ln}}\frac{I_l(\beta_{ln}R)}{K_l(q_{ln}R)}\right)^2\times\int_R^\infty d\rho\,\rho K_{|l|\pm1}^2(q_{ln}\rho)\right]^{1/2}. \tag{B3}$$

For fixed ω, ξ_{ln}, β_{ln}, and q_{ln} are uniquely determined from the characteristic equation

$$\frac{1}{\beta_{ln}R}\frac{I_{|l|\pm1}(\beta_{ln}R)}{I_{|l|}(\beta_{ln}R)}=\pm\frac{\varepsilon_0+1}{2\varepsilon_0}\Xi_{ln}'+\left[\frac{l}{(\beta_{ln}R)^2}-D_{ln}\right],$$

$$D_{ln}=\left[\left(\frac{\varepsilon_0-1}{2\varepsilon_0}\Xi_{ln}'\right)^2+l^2\left(\frac{c\xi_{ln}}{\omega}\right)^2\times\left[\frac{1}{(\beta_{ln}R)^2}+\frac{1}{(q_{ln}R)^2}\right]^2\frac{1}{\varepsilon_0}\right]^{1/2},$$

$$\Xi_{ln}=\frac{1}{(q_{ln}R)}\frac{K_l'(q_{ln}R)}{K_l(q_{ln}R)}. \tag{B4}$$

In these structures the fundamental mode is the HE_{11} mode.

At large radii modes are well confined in the internal region and the characteristic equation can be approximated as $I_{|l|\pm1}(\beta_{ln}R)=0$, giving transverse wave vectors $\beta_{ln}=x_{|l|\pm1,n}/R$ (x_{ln} is the nth root of the Bessel function of order l).

[1] G. H. Wannier, Phys. Rev. **100**, 1227 (1955); **101**, 1835 (1956); **117**, 432 (1960); Rev. Mod. Phys. **34**, 645 (1962).
[2] K. Leo, Semicond. Sci. Technol. **13**, 249 (1998).
[3] C. Waschke *et al.*, Phys. Rev. Lett. **70**, 3319 (1993); T. Dekorsky *et al.*, Phys. Rev. B **51**, R17 275 (1995).
[4] G. Nenciu, Rev. Mod. Phys. **63**, 91 (1991).
[5] F. Rossi *et al.*, Phys. Rev. B **51**, 16 943 (1995).
[6] F. Rossi, A. Di Carlo, and P. Lugli, Phys. Rev. Lett. **80**, 3348 (1998).
[7] A. Sibille, J. F. Palmier, and F. Laruelle, Phys. Rev. Lett. **80**, 4506 (1998).
[8] J. D. Joannopoulos, R. D. Meade, and J. N. Winn, *Photonic Crystals* (Princeton University Press, Princeton, NJ, 1995).
[9] J. N. Winn *et al.*, Phys. Rev. B **59**, 1551 (1999).
[10] G. Monsivais, M. del Castillo-Mussot, and F. Claro, Phys. Rev. Lett. **64**, 1433 (1990); C. Martijn de Sterke *et al.*, Phys. Rev. E **57**, 2365 (1998).
[11] A. Kavokin, G. Malpuech, A. Di Carlo, P. Lugli, and F. Rossi, Phys. Rev. B **61**, 4413 (2000).
[12] A. Yariv, *Optical Electronics* (Saunders College, San Francisco, 1991).
[13] G. Konotop, J. Opt. Soc. Am. B **14**, 364 (1997).
[14] N. S. Kapany and J. J. Burke, *Optical Waveguides* (Academic, New York, 1972).
[15] L. Pavesi, Riv. Nuovo Cimento **20**, 1 (1997).
[16] G. Malpuech and A. Kavokin, Semicond. Sci. Technol. (to be published).
[17] G. Panzarini *et al.*, Phys. Rev. B **59**, 5082 (1999), and references therein.
[18] J. M. Gérard *et al.*, Appl. Phys. Lett. **69**, 449 (1996).
[19] J. M. Gérard, B. Sermage, B. Gayral, B. Legrand, E. Costard, and V. Thierry-Mieg, Phys. Rev. Lett. **81**, 1110 (1998).